NASA Contractor Report 4434

P. 44

Computational Methods in the Prediction of Advanced Subsonic and Supersonic Propeller Induced Noise—ASSPIN Users' Manual

M. H. Dunn and G. M. Tarkenton

CONTRACT NAS1-19000
APRIL 1992

NASA Contractor Report 4434

Computational Methods in the Prediction of Advanced Subsonic and Supersonic Propeller Induced Noise—ASSPIN Users' Manual

M. H. Dunn and G. M. Tarkenton
Lockheed Engineering & Sciences Company
Hampton, Virginia

Prepared for
Langley Research Center
under CONTRACT NAS1-19000

NASA
National Aeronautics and
Space Administration
Office of Management
Scientific and Technical
Information Program
1992

CONTENTS

PRECEDING PAGE BLANK NOT FILMED

LIST OF FIGURES

LIST OF TABLES

SUMMARY

This document describes the computational aspects of propeller noise prediction in the time domain and the use of the high speed propeller noise prediction program **ASSPIN** (**A**dvanced **S**ubsonic and **S**upersonic **P**ropeller **I**nduced **N**oise). The code, which was formerly called the **DFP-ATP** (**D**unn-**F**arassat-**P**adula **A**dvanced **T**echnology **P**ropeller) noise prediction program, was developed at NASA Langley Research Center (LaRC) by the authors and F. Farassat and S. Padula of NASA LaRC. ASSPIN is the latest version of a sequence of propeller noise prediction codes that are based on the theoretical formulations of Farassat. These formulations are valid in both the near and far fields. Two such formulations are utilized by ASSPIN. One formulation is used for subsonic portions of the propeller blade, and the other for the transonic and supersonic regions. Switching between the formulations is performed automatically. ASSPIN incorporates advanced blade geometry and surface pressure modelling, adaptive observer time grid strategies, and relative to the previous version of the propeller noise prediction code, contains enhanced numerical algorithms that result in reduced computational time. In addition, the ability to treat the nonaxial inflow case has been included.

INTRODUCTION

Advanced Technology Propellers (ATP) or Propfans are a new generation of propellers that feature highly loaded blades that are thin and swept back (Figure 1). Propfan propelled aircraft are able to attain the same high speed, high altitude flight as current jet technology, but with a 20 to 25 percent reduction in fuel consumption (reference 1). Counter-rotating propfans (Figure 2) reduce swirl losses in the slipstream providing additional reduction in fuel consumption.

Producing blade designs that suppress propeller noise is an active area of research in the field of aeroacoustics. The construction and acoustical testing of new propeller designs is expensive and time consuming. Analytical methods, on the other hand, provide the engineer with a cost effective alternative to the experimental determination of propeller noise. This work is motivated by the need for an accurate analytical propeller noise prediction method that includes all computationally feasible physical effects.

ASSPIN is a computer program that predicts the noise generated by propellers operating at subsonic, transonic, or supersonic helical tip speeds in either single-rotation or counter-rotation mode. The prediction method is based on two theoretical time

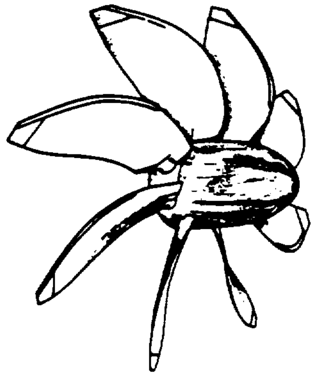

Figure 1. Single-Rotation Propeller

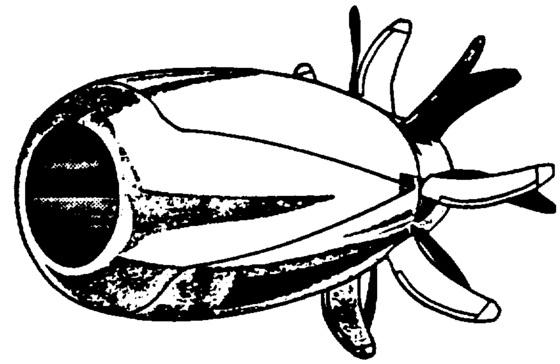

Figure 2. Counter-Rotating Propellers

domain formulations of Farassat (references 2,3). One formulation is valid for subsonic regions of a propeller blade, and the other, though valid for all speeds, is used only for transonic and supersonic portions of the blade. The formulations, without modification, apply in both the near and far fields, and to the nonaxial inflow case. Input to ASSPIN consists of blade kinematic and geometric quantities and either steady or periodically unsteady blade surface pressure. Program output includes propeller power and thrust coefficients, and the periodic acoustic signatures and acoustic spectra for the thickness, loading, and combined noise.

ASSPIN is the latest version of a sequence of noise prediction codes (references 4,5,6) that are based on the theoretical formulations of Farassat. Relative to the previous version of the code (reference 6), ASSPIN contains enhanced numerical and analytical methods that are designed to reduce computational time and increase accuracy. These facets of ASSPIN are explored in the Computational Strategy section.

ASSPIN has been used as part of a comprehensive propeller analysis package that includes state-of-the-art methods in propeller aeroacoustics, aerodynamics, and aeroelasticity. It has been demonstrated that acoustic results generated by ASSPIN within the propeller analysis code agree well with actual flight data (reference 7).

LIST OF SYMBOLS AND ABBREVIATIONS

A_1, A_2	reference frame rotation matrices
$\vec{b}$	$\lambda \vec{M}_t + \lambda_1 \vec{t}_1$; $b \equiv \left\|\vec{b}\right\|$
$\tilde{B}^i$	components of $\vec{b}$ in direction of blade principal curvatures, $i = 1, 2$

b_n	$\vec{b} \cdot \vec{n}$
CRP	counter-rotation propeller
c_0	speed of sound in undisturbed fluid
C_P	propeller power coefficient
C_T	propeller thrust coefficient
dB	decibels
dS	element of blade surface area
$f(\vec{y},\, \tau) = 0$	equation describing blade surface in reference frame fixed to undisturbed medium
$F(\vec{y};\, \vec{x},\, t)$	$f(\vec{y},\, t - r/c_0)$
H	local mean curvature of blade surface
h_n	$\lambda M_n + \lambda_1 \cos\theta$
$k(\vec{y},\, \tau)$	function defined so that the intersection of the surfaces $k = 0$ and $f = 0$ specifies the bounding curves of an open piece of the blade surface; intersection of the region $k > 0$ and the surface $f = 0$ defines an open piece of the blade surface
$K(\vec{y};\, \vec{x},\, t)$	$k(\vec{y},\, t - r/c_0)$
$\vec{M}$	local Mach vector based on c_0; $M \equiv \left\lvert \vec{M} \right\rvert$
$M_{a\nu}$	$\vec{M} \cdot \vec{\nu}$, $\vec{M}$ with respect to a medium fixed observer
$\dot{\vec{M}}$, $\dot{M}_i$	time derivative of $\vec{M}$
M_n	$\vec{M} \cdot \vec{n}$
M_r	$\vec{M} \cdot \hat{r}$
$\vec{M}_p$	projection of $\vec{M}$ onto local normal plane to blade surface edges; $M_p \equiv \left\lvert \vec{M}_p \right\rvert$
$\vec{M}_t$	projection of $\vec{M}$ onto local tangent plane to blade surface; $M_t \equiv \left\lvert \vec{M}_t \right\rvert$
$\vec{n}$, n_i	unit normal to blade surface
N_B	number of blades

p'	acoustic pressure
p	blade surface pressure expressed in medium fixed coordinates
$\dot{p}$	time derivative of p
p_B	blade surface pressure expressed in blade fixed coordinates
PCA	pitch change axis
Q	relative chord curvilinear coordinate
$\vec{r}$, r_i	$\vec{x} - \vec{y}$, $r \equiv \|\vec{r}\|$
$\hat{\vec{r}}$, $\hat{r}_i$	$\vec{r}/r$
$\hat{r}_\nu$	$\hat{\vec{r}} \cdot \vec{\nu}$
$\hat{\vec{r}}_p$	unit vector in the direction of the projection of $\vec{r}$ onto the local normal plane to the surface edges
SPL	sound pressure level
SRP	single-rotation propeller
t	observer time
$\vec{t}_1$	projection of $\hat{\vec{r}}$ onto local tangent plane to blade surface
V_F	forward flight velocity
$\vec{V}$	velocity vector
$\vec{x}$	observer position expressed in medium fixed coordinates
$\vec{y}$	source position expressed in medium fixed coordinates
$\vec{Y}$	source position expressed in aircraft fixed coordinates

Greek Symbols

α	inflow angle
$d\gamma$	elemental arc length along acoustic planform edges
$d\Gamma$	elemental arc length on curve formed by the intersection of the collapsing sphere and the moving blade for a fixed source time
δ	Dirac delta function
$d\Sigma$	element of acoustic planform area

θ	angle between $\vec{n}$ and $\vec{r}$
$\vec{\eta}$	blade surface point expressed in blade fixed coordinates
η_2	spanwise curvilinear coordinate
Λ	$\sqrt{1 + M_n^2 - 2M_n \cos\theta}$
$\tilde{\Lambda}$	$\sqrt{\Lambda^2 + \sin^2\theta}$
Λ_0	$\sqrt{M_p^2 \cos^2\theta + \left(1 - \vec{M}_p \cdot \hat{r}_p \sin\psi\right)^2}$
$\tilde{\mu}^i$	components of $\vec{M}_t$ in direction of principal curvatures, $i = 1, 2$
$\vec{\nu}$	local inward unit geodesic normal to the curve given by the intersection of the surfaces $k = 0$ and $f = 0$
ρ_0	density of undisturbed fluid
σ_b	length parameter along $\vec{b}$ on $f = 0$
σ_{11}, σ_{22}	two components of the tensor $\vec{t}_1\vec{t}_1 - \vec{M}\vec{t}_1$
τ	source time
ψ	angle between $\vec{r}$ and edge of surface given by the intersection of the surfaces $k = 0$ and $f = 0$
$\vec{\Omega}$, Ω_i	$\vec{n} \times \vec{\omega}$
κ_1, κ_2	local principal curvatures of the surface $f = 0$
κ_m, κ_t, κ_b	local normal curvatures of the surface $f = 0$ in the direction of $\vec{M}_t$, $\vec{t}_1$, and $\vec{b}$, respectively
λ	$\dfrac{\cos\theta - M_n}{\tilde{\Lambda}^2}$
λ_1	$\dfrac{\cos\theta + M_n}{\tilde{\Lambda}^2}$
$\vec{\chi}$	observer position expressed in blade fixed coordinates
$\vec{\omega}$	angular velocity; $\omega \equiv \lvert\vec{\omega}\rvert$

THEORETICAL FORMULATIONS

Small perturbations in fluid quantities due to the motion of a body through an otherwise quiescent, ideal fluid are governed by the equations of linearized acoustics.

Therefore, in the region exterior to the body, the acoustic pressure, $p'(\vec{x}, t)$, is a solution of the homogeneous wave equation subject to the boundary condition that the fluid cannot penetrate the surface of the body.

Using generalized function theory, the restricted domain of the above problem, *i.e.*, the body's exterior, can be extended to include the entirety of space by the process of embedding (reference 8). Applying this procedure to the equations of linearized acoustics leads to the Ffowcs Williams-Hawkings equation without the quadrupole term (reference 9):

$$\frac{1}{c_0^2}\frac{\bar{\partial}^2 p'}{\partial t^2} - \bar{\nabla}^2 p' = \bar{\nabla}_4 \cdot \left[\vec{Q}\ |\nabla f|\ \delta(f)\right], \tag{1}$$

where

$$\bar{\nabla}_4 \equiv \left(\bar{\nabla},\ \frac{1}{c_0}\frac{\bar{\partial}}{\partial t}\right), \quad \vec{Q} \equiv (-p\vec{n},\ M_n),$$

and the bars over the differential operators denote generalized differentiation (reference 8). The boundary condition and the pressure on the surface of the body appear as source terms in (1). The advantage of the embedding technique is that the Green's function for the wave equation in unbounded space is known, thus the solution of (1) can be obtained analytically provided the aerodynamic pressure on the surface of the body is known.

There are several different ways to express the solution of (1). Two forms of the solution are particularly effective for numerical evaluation and are considered here. The first form, known as **Formulation 1A** (reference 2), is valid over source regions that move toward the observer point, $\vec{x}$, at subsonic speed. The second form of the solution is referred to as **Formulation 3** (reference 3). Formulation 3 is valid for the entire body regardless of its speed, but for computational reasons that are discussed later in this section it is used only for supersonic and transonic portions of the body. In the subsequent discussions, the acoustic pressure will be written as

$$p'(\vec{x},\ t) = p'_T(\vec{x},\ t) + p'_L(\vec{x},\ t),$$

where p'_T and p'_L are referred to as the thickness and loading noise components, respectively.

For Formulation 1A, the acoustic pressure components are written in terms of surface integrals over the moving body as follows:

$$4\pi p'_T(\vec{x},\, t) = c_0 \rho_0 \int\limits_{f=0} \left[\frac{M_n \left(r\dot{M}_i \hat{r}_i + c_0 M_r - c_0 M^2 \right)}{r^2 \left(1 - M_r\right)^3} \right]_{ret} dS, \tag{2a}$$

and

$$\begin{aligned} 4\pi p'_L(\vec{x},\, t) =& \frac{1}{c_0} \int\limits_{f=0} \left[\frac{\dot{p}\cos\theta}{r\left(1 - M_r\right)^2} \right]_{ret} dS + \int\limits_{f=0} \left[\frac{p\left(\cos\theta - M_n\right)}{r^2 \left(1 - M_r\right)^2} \right]_{ret} dS \\ &+ \frac{1}{c_0} \int\limits_{f=0} \left[\frac{p\cos\theta \left(r\dot{M}_i \hat{r}_i + c_0 M_r - c_0 M^2 \right)}{r^2 \left(1 - M_r\right)^3} \right]_{ret} dS. \end{aligned} \tag{2b}$$

The subscript $_{ret}$ appearing in the above formulae implies that the integrands are to be evaluated at the retarded (or emission) time $t - r/c_0$. Observe that evaluation of (2a) and (2b) involves the calculation of kinematic, geometric, and aerodynamic quantities on the surface of the moving body. In particular, note that the geometric quantities required to evaluate (2a) and (2b) depend on the mathematical surface representation (*viz.* r, M_r, $\hat{r}_i$, and $f = 0$) and it's first derivatives (*viz.* M_n, θ, and dS).

Portions of the body that move toward the observer at transonic or supersonic speed require a different formulation than the above. This is because the Doppler factor, $1 - M_r$, appearing in (2a) and (2b) becomes small at transonic speeds relative to the observer, rendering the integrals improper. Consequently, the analysis upon which these equations are based is invalid. With minor modifications, (2a) and (2b) are valid for strictly supersonic regions of the moving body. However, experience has shown that it is computationally difficult to differentiate between 'nearly' transonic and supersonic source regions. These considerations prompted the development of Formulation 3 which, as previously mentioned, is mathematically valid for all flight regimes. In contrast to Formulation 1A, Formulation 3 is written in terms of surface integrals over open portions of the acoustic planform surface and line integrals over the edges of the open portions. The acoustic planform is generated by open portions of the moving surface (a panel, for example). Using Formulation 3, the thickness and loading components of the acoustic pressure can be written as

$$\frac{4\pi}{\rho_0 c_0^2} p'_T(\vec{x},\, t) = \int\limits_{\substack{F=0\\K>0}} \frac{1}{r^2}\left[\frac{M_n^2 Q'_N}{\Lambda}\right]_{ret} d\Sigma + \int\limits_{\substack{F=0\\K>0}} \frac{1}{r}\left[\frac{M_n^2 Q_F + Q'_F + Q''_F}{\Lambda}\right]_{ret} d\Sigma$$
$$- \int\limits_{\substack{F=0\\K=0}} \frac{1}{r}\left[\frac{M_n^2 Q_E + M_n M_{a\nu}}{\Lambda_0}\right]_{ret} d\gamma, \qquad (3a)$$

and

$$4\pi p'_L(\vec{x},\, t) = \int\limits_{\substack{F=0\\K>0}} \frac{1}{r^2}\left[\frac{pQ'_N}{\Lambda}\right]_{ret} d\Sigma + \int\limits_{\substack{F=0\\K>0}} \frac{1}{r}\left[\frac{pQ_F + \frac{\lambda}{c_0}\dot{p}_B - b\frac{\partial p_B}{\partial \sigma_b}}{\Lambda}\right]_{ret} d\Sigma$$
$$- \int\limits_{\substack{F=0\\K=0}} \frac{1}{r}\left[\frac{pQ_E}{\Lambda_0}\right]_{ret} d\gamma, \qquad (3b)$$

respectively, where

$$Q'_N = \lambda\left[2\lambda_1 (\cos\theta - M_n) + 1\right],$$

$$\begin{aligned} Q_F =& \frac{1}{c_0}\left(2\lambda^2 - \frac{1}{\tilde{\Lambda}^2}\right)\dot{M}_n + 2b^2\kappa_b + \kappa_1\sigma_{11} + \kappa_2\sigma_{22} - 2Hh_n \\ &+ \frac{1}{c_0}\vec{\Omega}\cdot\left[\frac{\vec{M}_t - \vec{t}_1}{\tilde{\Lambda}^2} - 2\lambda\vec{b} + \left(\frac{1}{\tilde{\Lambda}^2} + 2\lambda\lambda_1\right)\vec{\hat{r}}\right], \end{aligned}$$

$$Q'_F = 2M_n\left[\frac{1}{c_0}\left(\lambda\dot{M}_n - \vec{\Omega}\cdot\vec{b}\right) + \kappa_1\tilde{\mu}^1\tilde{B}^1 + \kappa_2\tilde{\mu}^2\tilde{B}^2\right],$$

$$Q''_F = \frac{1}{c_0}\left(\dot{M}_n - \vec{\Omega}\cdot\vec{M}_t\right) + \kappa_m M_t^2 - 2HM_n^2,$$

and

$$Q_E = \lambda M_{a\nu} + \lambda_1\hat{r}_\nu.$$

In equations (3a) and (3b), the notation $F = 0$, $K > 0$, defines an open piece of the acoustic planform surface, and $F = 0$, $K = 0$ defines its boundary. The quantities F and K are defined by

$$F(\vec{y};\, \vec{x},\, t) = f(\vec{y},\, t - r/c_0) \quad \text{and} \quad K(\vec{y};\, \vec{x},\, t) = k(\vec{y},\, t - r/c_0),$$

with $f = 0$, $k > 0$ defining an open portion of the moving surface and $f = 0$, $k = 0$ its boundary.

The acoustic planform (or Σ surface) is a surface in space generated by the intersection of the surface of the moving body and a sphere, centered at $\vec{x}$, whose radius collapses at the speed of sound to the point $\vec{x}$ at the time t. In practice, the surface integrals of (3a) and (3b) are best calculated by the so called collapsing sphere method (reference 10), in which the relation

$$\frac{d\Sigma}{\Lambda} = \frac{c_0 \, d\Gamma d\tau}{\sin\theta} \tag{4}$$

is utilized. In (4), the source time integration is over the period(s) of time in which the collapsing sphere, given by the equation

$$\frac{|\vec{x} - \vec{y}|}{c_0} = t - \tau \tag{5}$$

and the moving body, represented by $f(\vec{y}, \tau) = 0$, intersect. For fixed τ, $d\Gamma$ denotes elemental arc length along the curve(s) of intersection of the collapsing sphere and the moving body.

Similar to the integrands of Formulation 1A, the evaluation of (3a) and (3b) involves the calculation of geometric, kinematic, and aerodynamic quantities. However, the integrands of Formulation 3 contain many more terms than those of (2a) and (2b). Furthermore, second derivatives of the mathematical surface representation must be computed. This is because the terms Q_F, Q'_F, and Q''_F contain curvature information about the surface of the moving body. For these reasons, Formulation 3 is used only for the transonic and supersonic regions of the moving body even though it is valid everywhere.

COMPUTATIONAL STRATEGY

In this section, the computational strategies for applying equations (2), (3), and (4) to propeller noise predictions are discussed. The section is composed of several subsections which highlight various analytical and computational facets of the solution procedure.

Blade and Surface Pressure Modelling

Calculations with ASSPIN begin by modelling user supplied blade geometry and loading data with high order, tensor product, least-squares splines. The modelling is performed automatically by a modified version of the software appearing in reference 12. Blade surface parameterization involves representing the Cartesian coordinates of blade points in terms of spanwise, η_2, and percentage chord, Q, curvilinear coordinates. Steady blade loads are parameterized in a similar fashion. The resulting two dimensional surface functions are easily evaluated and differentiated as required by the integrands of (2) and (3).

Unsteady blade surface pressure due to nonaxial inflow is periodic with period $2\pi/\omega$, where ω is the angular speed of the propeller. At each user defined blade point, unsteady pressure is input as a function of time over the entire period of revolution. To evaluate the unsteady pressure and its derivatives as required by ASSPIN, the Fourier time series of the unsteady blade surface pressure is computed. The Fourier coefficients, which are functions of the blade curvilinear coordinates η_2 and Q, are stored and interpolated as required. At present, ASSPIN computes the first five components of the Fourier series. If there are regions of time in which the surface pressure varies rapidly, for example if there is a pylon in front of the propeller, then additional Fourier components may be required for adequate representation. In these cases, ASSPIN can be easily modified to accommodate the increased resolution.

Previous versions of the noise prediction code evaluated the unsteady surface pressure by straightforward three dimensional interpolation. Compared to steady surface pressure noise predictions, predictions in which unsteady loading was required used excessive amounts of computer time. This problem has been alleviated by the incorporation of the above strategy in which evaluation of the unsteady pressure has been reduced to a two dimensional interpolation problem. Unsteady surface pressure noise predictions now require only 1.25 times the execution time of steady surface pressure predictions.

Coordinate Reference Frames

There are three Cartesian reference frames used in the noise calculations. They are the medium fixed $\vec{x}$-frame, the aircraft fixed $\vec{X}$-frame, and the blade fixed $\vec{\eta}$-frame (Figure 3). Initially, it is assumed that the propeller center is at the origin of the $\vec{x}$-frame. The x_3 axis lies in the direction of flight, with positive x_3 pointing in the direction of motion. The directions x_1 and x_2 are defined so that the $\vec{x}$-frame is right-handed. The aircraft fixed frame is identical to the medium fixed frame initially and moves in the forward flight direction with speed V_F.

The origin of the blade fixed frame coincides with the origin of the aircraft fixed frame at all times. The angle between the η_3 axis and the x_3 (or X_3) axis is the inflow angle, α. The pitch change axis of the propeller blade always lies along the η_2 axis, and η_1 is chosen so that the $\vec{\eta}$ frame is right handed. Note that if the inflow angle is zero, then the η_3 axis and the X_3 axis always coincide. For single rotating propellers and the forward propeller of CRPs, the blade is assumed to rotate counterclockwise in the $\eta_1\eta_2$-plane with respect to an observer looking down the η_3 axis. The aft propeller of CRPs is assumed to rotate clockwise.

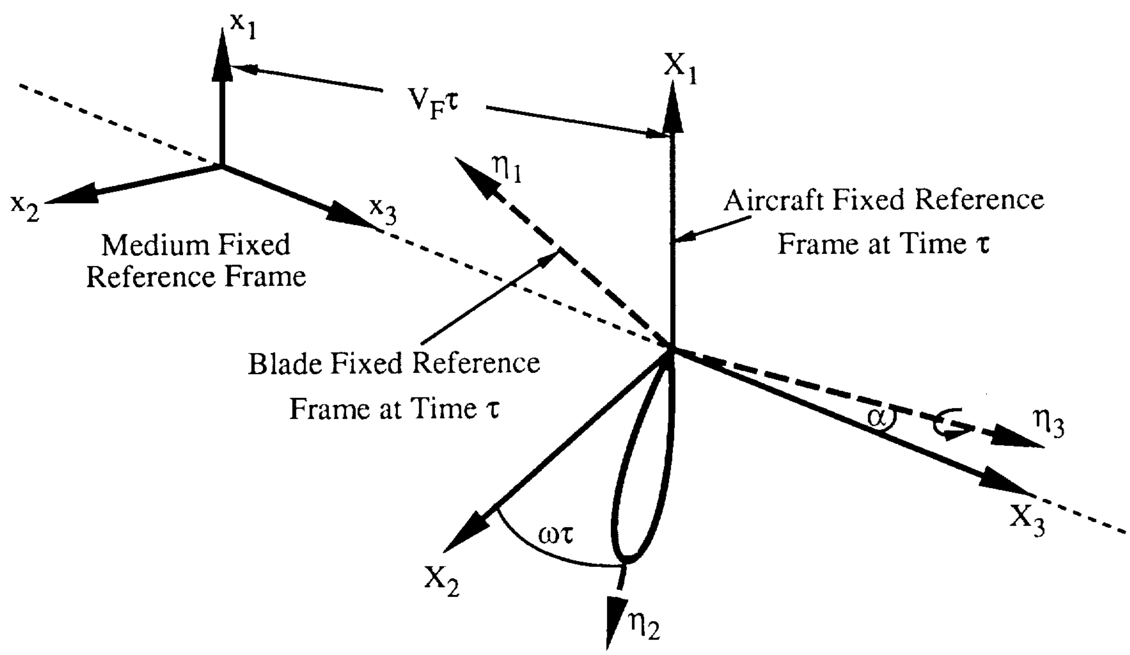

Figure 3. ASSPIN Reference Frames

The mathematical relationships between the three reference frames are obtained by applying the appropriate translations and rotations. Let $\vec{\eta}$ denote the blade fixed coordinates of an arbitrary blade point. At time τ, let $\vec{y}(\tau)$ and $\vec{Y}(\tau)$ represent the locations of the moving blade point in medium fixed coordinates and aircraft fixed coordinates, respectively. If ω is the angular speed of the propeller, then the following relations exist:

$$\vec{y}(\tau) = \vec{Y}(\tau) + \begin{pmatrix} 0 \\ 0 \\ V_F\tau \end{pmatrix} \tag{6}$$

and

$$\vec{Y}(\tau) = A_1 A_2(\tau)\vec{\eta}, \tag{7}$$

where A_1 and $A_2(\tau)$ are the 3×3 rotation matrices

$$A_1 = \begin{pmatrix} \cos\alpha & 0 & -\sin\alpha \\ 0 & 1 & 0 \\ \sin\alpha & 0 & \cos\alpha \end{pmatrix}$$

and

$$A_2(\tau) = \begin{pmatrix} \cos\omega\tau & -\sin\omega\tau & 0 \\ \sin\omega\tau & \cos\omega\tau & 0 \\ 0 & 0 & 1 \end{pmatrix}.$$

The velocity, $\vec{V}(\tau)$, of a blade point with respect to an observer in the medium fixed frame is obtained by differentiating (6) with respect to source time. Thus,

$$\vec{V}(\tau) = \frac{\partial \vec{y}(\tau)}{\partial \tau} = A_1 \frac{\partial A_2(\tau)}{\partial \tau} \vec{\eta} + \begin{pmatrix} 0 \\ 0 \\ V_F \end{pmatrix}, \tag{8}$$

where

$$\frac{\partial A_2(\tau)}{\partial \tau} = \omega \begin{pmatrix} -\sin\omega\tau & -\cos\omega\tau & 0 \\ \cos\omega\tau & -\sin\omega\tau & 0 \\ 0 & 0 & 0 \end{pmatrix}.$$

In order for the integrands of (2) and (3) to be meaningful, all of the terms must be written in the same coordinate system. Most of the terms contain only blade geometric quantities. These quantities are easily computed in terms of blade fixed coordinates by evaluating the spline functions that were described in the previous subsection. Therefore, to facilitate the evaluation of the integrands, all terms that involve vector operations (*e.g.*, dot products) are expressed in blade fixed coordinates. It is natural to write the Mach vector, $\vec{M}$, of a blade point and the moving observer point, $\vec{x}$, in medium fixed coordinates. Thus, $\vec{M}$ and $\vec{x}$ must be expressed in blade fixed coordinates in order to maintain consistency.

The Mach vector, expressed in terms of medium fixed coordinates, is obtained from (8). Since $\vec{M}$ is viewed as a free vector, it follows that its representation with respect to the aircraft fixed frame is the same as that of the medium fixed frame. Consequently, at time τ, the Mach vector of a moving blade point, $\vec{\eta}$, expressed in blade fixed coordinates is calculated by applying the inverse transformation of (7) to equation (8) which yields

$$\vec{M}(\tau) = \frac{1}{c_0} A_2^{-1}(\tau) A_1^{-1} \frac{\partial \vec{y}(\tau)}{\partial \tau} = \frac{1}{c_0} A_2^{-1}(\tau) \frac{\partial A_2(\tau)}{\partial \tau} \vec{\eta} + A_2^{-1}(\tau) A_1^{-1} \begin{pmatrix} 0 \\ 0 \\ M_F \end{pmatrix}, \tag{9}$$

where

$$A_2^{-1}(\tau) = \begin{pmatrix} \cos\omega\tau & \sin\omega\tau & 0 \\ -\sin\omega\tau & \cos\omega\tau & 0 \\ 0 & 0 & 1 \end{pmatrix},$$

and

$$A_1^{-1} = \begin{pmatrix} \cos\alpha & 0 & \sin\alpha \\ 0 & 1 & 0 \\ -\sin\alpha & 0 & \cos\alpha \end{pmatrix}.$$

Consider an observer point that moves with the aircraft. Suppose that the initial position of the observer with respect to the medium fixed frame is given by $(x_1,\ x_2,\ x_3)$. At the observer time t, the observer point has translated $V_F t$ distance units in the x_3 direction. Therefore, the coordinates of the observer point at time t with respect to the aircraft fixed frame at the source time τ are $(x_1,\ x_2,\ x_3 + V_F\,(t-\tau))$. Thus, the location of the observer with respect to the blade fixed frame, $\vec{\chi}(t;\ \tau)$, is given by

$$\vec{\chi}(t;\ \tau) = A_2^{-1}(\tau)A_1^{-1} \begin{pmatrix} x_1 \\ x_2 \\ x_3 + V_F\,(t-\tau) \end{pmatrix}. \tag{10}$$

Let $\vec{\eta}$ be the blade fixed coordinates of a blade surface point, and let τ be the source (emission or retarded) time, then, according to equation (10), the radiation vector, $\vec{r}$, appearing in equations (2) and (3) can expressed in terms of blade fixed coordinates as

$$\vec{r} = \vec{\chi}(t,\ \tau) - \vec{\eta}. \tag{11}$$

Retarded Time Calculation

Computations with either Formulation 1A or Formulation 3 involve the repeated calculation of retarded (or emission) times. For fixed observer position, $\vec{x}$, and observer time, t, the retarded time, τ, is a solution of the retarded time equation (RTE)

$$|\vec{r}| = |\vec{x}(t) - \vec{y}(\tau)| = c_0\,(t-\tau), \tag{12}$$

where $\vec{y}$ is a fixed source point whose emission time(s) are sought. Equation (12) states that an acoustic signal, traveling at the speed of sound, that leaves $\vec{y}$ at time τ takes $t-\tau$ time units to reach the observer position $\vec{x}$ at time t. It can be shown (reference 13) that the RTE has exactly one solution for subsonic motion between source and observer. However, if the relative motion is supersonic, then the RTE may have many solutions. At current design conditions, propfans operate at helical tip speeds of about 1.15. It has been found that the RTE has at most three solutions at these speeds.

For a typical supersonic helical tip speed case, retarded time calculations account for approximately 50% of ASSPIN's total computational time. Furthermore, since the theoretical formulations require accurate retarded times to be useful, a robust algorithm for solving the RTE is necessary. In the ensuing discussion, the precise form of the RTE for propeller motion is developed, and an efficient method for finding its roots is presented.

Suppose (η_1, η_2, η_3) are the blade fixed coordinates of a blade point and (x_1, x_2, x_3) are the initial coordinates, with respect to the medium fixed frame, of an observer point. If t is the observer time, then the RTE can be combined with equation (11) to yield

$$\vec{r}\cdot\vec{r} = |\vec{X}(t;\,\tau) - \vec{\eta}|^2 = c_0^2\,(t-\tau)^2\,. \tag{13}$$

Let

$$\begin{aligned}
\phi &= \omega\,(\tau - t)\,,\\
x_1^* &= x_1\cos\alpha + x_3\sin\alpha,\\
x_2^* &= x_2,\\
x_3^* &= x_3\cos\alpha - x_1\sin\alpha,\\
x^* &= \sqrt{x_1^{*2} + x_2^{*2}},\\
\eta &= \sqrt{\eta_1^2 + \eta_2^2},\\
\psi_x &= \tan^{-1}\frac{x_2^*}{x_1^*},
\end{aligned}$$

and

$$\psi_\eta = \tan^{-1}\frac{\eta_2}{\eta_1},$$

then equation (13) can be written

$$A\phi^2 + B\phi + C + \cos(\phi + D) + E\phi\sin(\phi + F) = 0, \tag{14}$$

where

$$
\begin{aligned}
A =& \frac{c_0^2 - V_F^2}{2\eta x^* \omega^2}, \\
B =& \frac{V_F\left[x_1^* \sin\alpha + \left(x_3^* - \eta_3\right)\cos\alpha\right]}{\omega\eta x^*}, \\
C =& -\frac{\left[x^{*2} + \eta^2 + \left(x_3^* - \eta_3\right)^2\right]}{\omega\eta x^*}, \\
D =& \psi_\eta - \psi_x + \omega t, \\
E =& -\frac{V_F \sin\alpha}{\omega x^*}, \quad \text{and} \\
F =& \psi_\eta + \omega t.
\end{aligned}
$$

Equation (14) is an implicit, transcendental equation for ϕ which cannot be solved analytically. Further complications arise when the motion of the source point toward the observer is supersonic. In this instance, (14) has multiple solutions and straightforward root finding algorithms, such as Newton's method, must be augmented by analysis if all roots are to be resolved. A robust algorithm for finding all roots of the RTE has been developed by the authors and is discussed below.

Since equation (14) was obtained by squaring equation (12), it follows that spurious solutions of (14) might exist. This problem is resolved by enforcing the causality condition, which states that a signal must be emitted before it can be observed. Thus, if ϕ^* is a solution of (14), then it must satisfy the relation

$$
\operatorname{sgn}(\omega)\phi^* \leq 0. \tag{15}
$$

This is because $\phi = \omega(\tau - t)$, and τ must be less than or equal to t if the causality condition is to be satisfied.

Let $g(\phi)$ denote the left hand side of (14). Equation (15) gives limited information on where to search for roots of g. However, sharp bounds can be obtained by analyzing (14). It can be shown that

$$
\cos(\phi + D) + E\phi\sin(\phi + F) = \sqrt{E_1^2\phi^2 + (1 + E_2\phi)^2}\cos(\phi + D - \psi),
$$

where

$$
\begin{aligned}
E_1 &= E\cos\psi_x, \\
E_2 &= E\sin\psi_x, \quad \text{and} \\
\psi &= \tan^{-1}\frac{E_1\phi}{1 + E_2\phi}.
\end{aligned}
$$

Therefore, (14) can be written as

$$\frac{A\phi^2 + B\phi + C}{\sqrt{E_1^2\phi^2 + (1 + E_2\phi)^2}} = -\cos(\phi + D - \psi).$$

In absolute value, the right hand side of the above equation is bounded by one. Thus,

$$\left| \frac{A\phi^2 + B\phi + C}{\sqrt{E_1^2\phi^2 + (1 + E_2\phi)^2}} \right| \leq 1 \quad \text{for all} \quad \phi.$$

The roots of g that satisfy (15) are therefore bounded by the roots of

$$\left(A\phi^2 + B\phi + C\right)^2 = E_1^2\phi^2 + (1 + E_2\phi)^2 . \tag{16}$$

Equation (16) is a polynomial equation of degree four, whose roots are easily calculated. ASSPIN uses the computer program RPOLY, taken from reference 14, to solve (16). If ϕ^*_{min} and ϕ^*_{max} are the two solutions of (15) and (16), and if $\phi^*_{min} < \phi^*_{max}$, then any roots of g must lie in the interval $[\phi^*_{min}, \phi^*_{max}]$.

The next step in the root finding process involves the approximation of $g(\phi)$ on $[\phi^*_{min}, \phi^*_{max}]$ by a polynomial of degree three. The function g is evaluated at four evenly spaced points on $[\phi^*_{min}, \phi^*_{max}]$ and the interpolating cubic polynomial calculated. Any extreme points on $[\phi^*_{min}, \phi^*_{max}]$ of the cubic polynomial are then computed analytically. If extreme points exist, then they are used as initial guesses for finding the extreme points, if any, of g by Newton's method. If extreme points of g are discovered, then the cubic polynomial is recalculated by replacing some of the original interpolation points by the extreme points. The advantage of this last step is discussed below.

The final phase in the calculation of retarded times is to find the roots of the third degree polynomial analytically. Roots of the polynomial which lie in $[\phi^*_{min}, \phi^*_{max}]$ are then used as initial guesses to Newton's method for determining the roots of g.

It is difficult to distinguish between two roots that lie close together. Trying to resolve such roots using Newton's method requires accurate guesses for the initial iterants. Otherwise, Newton's method may diverge or keep converging to the same root. Two roots of a smooth function are separated by an extreme point. Therefore, using extreme points of g as interpolation points for the cubic polynomial enhances the approximation of g in the neighborhood of the adjacent roots. Consequently, if the roots of the cubic near an extreme point of g are used as initial guesses, then Newton's method converges rapidly to the nearest roots of g. This technique ensures that the search for all roots of the RTE is exhaustive.

Spectral Analysis

For a given observer point, $\vec{x}$, translating with the propeller, the periodic acoustic signature generated by a propeller with N_B blades is obtained by the superposition of the acoustic pressure signatures produced by the individual blades. If the blades are identical and symmetrically spaced and if $p_1'(\vec{x}, t)$ is the signature of one of the blades, then the cumulative pressure signal is given by

$$p'(\vec{x}, t) = \sum_{n=1}^{N_B} p_1'\left(\vec{x}, t + \frac{2\pi(n-1)}{N_B \omega}\right).$$

For each observer location, ASSPIN calculates p_1' at a discrete number of equally spaced time points, and applies the above formula to obtain the combined acoustic signature.

Before proceeding to the details of how p_1' is calculated, the spectral analysis of p' is considered. Acoustic output from ASSPIN consists of discrete pressure signatures for the loading, thickness, and combined noise, and the sound pressure levels as a function of harmonic number for each noise component. The temporal Fourier series of the acoustic pressure can be written

$$p'(\vec{x}, t) = \sum_{n=0}^{\infty} a_n(\vec{x}) \cos \omega_n t + b_n(\vec{x}) \sin \omega_n t,$$

where $\omega_n = nN_B\omega$. The Fourier coefficients are given by

$$a_n(\vec{x}) = \frac{2}{T} \int_0^T p'(\vec{x}, t) \cos \omega_n t dt, \tag{17a}$$

and

$$b_n(\vec{x}) = \frac{2}{T} \int_0^T p'(\vec{x}, t) \sin \omega_n t dt, \tag{17b}$$

where $T = \dfrac{2\pi}{N_B \omega}$.

Since p' is known for a discrete number of observer time points, equations (17a) and (17b) must be evaluated numerically. ASSPIN computes the Fourier coefficients by Simpson's rule (reference 11). Simpson's rule provides a higher degree of accuracy than Fast Fourier Transform (FFT) methods and is not limited to a specific number of time points (*viz.* 2^k for some k). As a result, greater flexibility and a higher degree of accuracy is attained relative to FFT methods. It is also worth mentioning here that the additional computational time required by Simpson's rule is negligible relative to the entire noise prediction process.

The n-th sound pressure level for the total acoustic pressure, SPL_n, is defined by the equation

$$SPL_n = 10 \log_{10} \frac{a_n^2(\vec{x}) + b_n^2(\vec{x})}{p_{ref}^2},$$

where $p_{ref} = 2 \times 10^{-5}$ Pascals is the reference pressure. Sound pressure levels for the thickness and loading components of the noise are defined similarly.

Discretization and Numerical Integration

The blade surface is separated into two regions - the subsonic root region and the transonic/supersonic tip region. The spanwise location

$$\eta_2^* = \frac{\mathrm{sgn}(\omega)}{\omega} \left(\sqrt{c_*^2 - V_F^2 \cos^2 \alpha} - V_F \sin \alpha \right),$$

where $c_* = (1 - \epsilon)c_0$ with ϵ a small user supplied parameter and α is the inflow angle, serves as the boundary separating the two regions. This separation point insures that the high speed portion of the blade, which might require the use of Formulation 3 to evaluate the noise contribution, is adequately disjoined from the subsonic region. Both regions are then subdivided into equally spaced spanwise and percent chord intervals according to user specifications which results in a panelled discretization (Figure 4a).

For a specified observer point, $\vec{x}$, the one blade periodic acoustic pressure signal, $p_1'(\vec{x}, t)$, is calculated at a discrete number of observer time points comprising the period of revolution for one blade. For this purpose, an adaptive observer time grid is employed. The adaptive grid is a function of observer location, operating conditions, and source geometry. To facilitate the spectral analysis of the acoustic signals, the results for the adaptive observer time grid are interpolated onto an evenly spaced observer time grid at the end of the calculations.

The idea behind the adaptive grid strategy is to determine the range of observer times (if such a range exists) in which blade points have multiple emission times. For

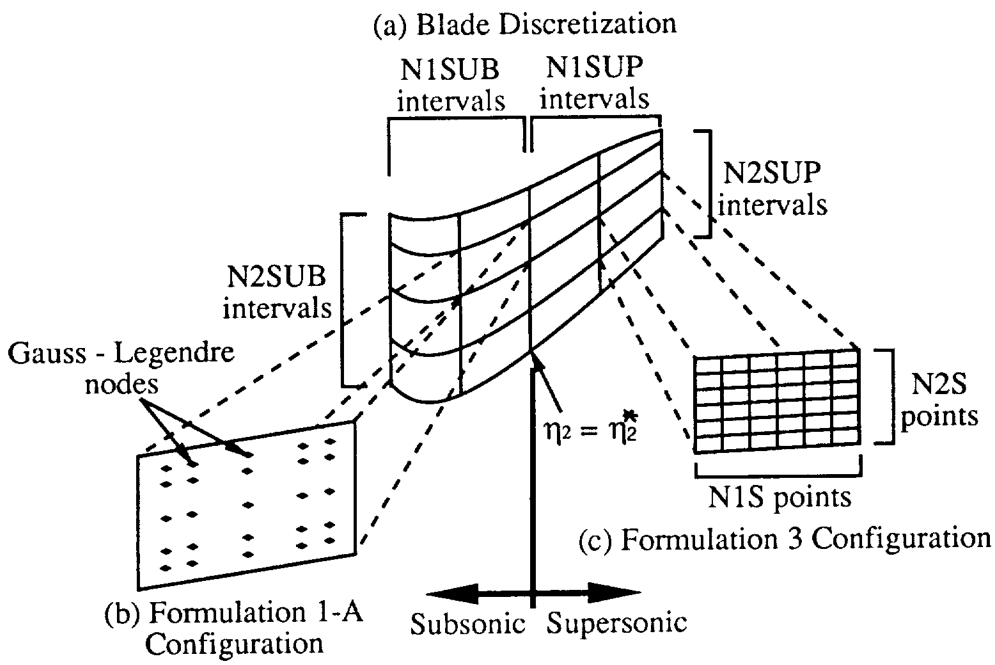

Figure 4. ASSPIN Computational Grids

observer times within this range, the panel contains transonic and/or supersonic sources requiring the use of Formulation 3. Panel sources are subsonic for observer times outside of the range, and the acoustic pressure for the panel at these observer times can be computed with Formulation 1A.

The range of observer times in which a fixed observer/source point pair has multiple emission times can be found by analyzing equation (14). Again denote the left hand side of (14) by the function $g(\phi)$. The coefficients D and F of (14) are functions of observer time, therefore the solution(s), ϕ, of $g(\phi) = 0$ is a function of t. A typical example of this functional dependence is shown below in Figure 5. In this illustration, a situation is depicted in which the RTE has multiple solutions when $t \in [t_{min}, t_{max}]$.

From Figure 5, observe that

$$\frac{d\phi}{dt} \to \infty \quad \text{at} \quad t = t_{min} \quad \text{and} \quad t = t_{max}. \tag{18}$$

Differentiating (14) with respect to t yields

$$\frac{d\phi}{dt} = \omega \frac{\sin(\phi + D) - E\phi\cos(\phi + F)}{2A\phi + B - \sin(\phi + D) + E\sin(\phi + F) + E\phi\cos(\phi + F)}.$$

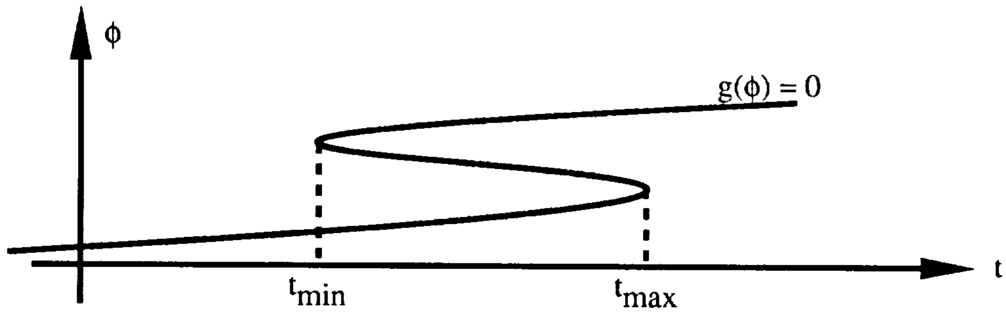

Figure 5. Multiple Emission Time Illustration

Therefore, it follows from (18) that

$$2A\phi + B - \sin(\phi + D) + E\sin(\phi + F) + E\phi\cos(\phi + F) = 0 \tag{19}$$

at $t = t_{min}$ and t_{max}.

The observer times t_{min} and t_{max} are obtained by solving equations (14) and (19) simultaneously for t and ϕ. It can be shown that the observer time can be eliminated from (14) and (19) resulting in the equation

$$\begin{aligned}
&\left[(E\phi + \sin\psi_x)\left(A\phi^2 + B\phi + C\right) - \cos\psi_x\,(2A\phi + B)\right]^2 \\
&+ \left[(\cos\psi_x - E)\left(A\phi^2 + B\phi + C\right) + (E\phi + \sin\psi_x)(2A\phi + B)\right]^2 \\
&= \left[\cos\psi_x\,(\cos\psi_x - E) + (E\phi + \sin\psi_x)^2\right]^2.
\end{aligned} \tag{20}$$

Equation (20) is a sixth degree polynomial in ϕ and ASSPIN finds its roots with RPOLY. The solutions of (20) that do not satisfy (15) are discarded and the observer times t_{min} and t_{max} are then found with either (14) or (19). This procedure is repeated for many source points on the blade. The final adaptive observer time grid for the blade is based on the minimum t_{min} and maximum t_{max} of all source points tested.

The acoustic pressure, when viewed as a function of observer time, has steep gradients in regions of observer time in which the blade sources emit signals that approach the observer at transonic or supersonic speed. For this reason, the period of time in which the blade contains points that have multiple emission times is finely discretized. Conversely, the observer time period in which the blade exhibits subsonic behavior is coarsely discretized.

The adaptive observer time grid strategy is a novel feature for high speed propeller noise prediction in the time domain. Its implementation in ASSPIN has reduced computer execution time by approximately 50 percent relative to previous versions of the noise prediction codes.

Consider a fixed panel on the discretized propeller blade. For a fixed observer point $\vec{x}$, the acoustic signal generated by the source panel is computed by looping through the adaptive observer time grid. For each observer time point of the adaptive grid, ASSPIN determines if the noise contribution for the panel is to be computed by Formulation 1A or Formulation 3. If the condition

$$(1 - M_r)_{ret} < \epsilon, \quad \epsilon \text{ prescribed}$$

is satisfied at some source point, then Formulation 3 is used for the panel at that observer time. Switching back and forth between the formulations is performed automatically. This procedure is repeated for each blade panel and the resulting acoustic signals summed.

If Formulation 1A is to be used, then the integrals of (2a) and (2b) are computed via Gauss-Legendre (G-L) quadrature (reference 11). A user prescribed number of G-L nodes and weights are calculated as part of ASSPIN preprocessing. The nodes are distributed over the panel (Figure 4b), and the integrands of (2a) and (2b) are evaluated at the nodes and summed according to G-L integration requirements.

Due to the complex nature of the integrands of (3a) and (3b), a simpler numerical quadrature scheme is employed for calculating Formulation 3 integrals. The Γ curves of equation (4) and the acoustic planform boundaries are approximated by piecewise straight lines and the integrals of (3a) and (3b) calculated by the trapezoidal rule (reference 11). Increased resolution is obtained by a further subdivision of the panel (see Figure 4c) according to user specifications.

The evaluation of the Formulation 3 surface integrals by the collapsing sphere method is a multiphase process. First, for a fixed observer time, the retarded times are computed at each vertex of the spatially refined panel. For each subdivided panel (refer to Figure 4c) the retarded times at the vertices are sorted in ascending order. Thus, the period of time in which the collapsing sphere intersects a particular panel is established. This period of source time is then discretized and the Γ curve, *i.e.*, the intersection of the panel and the collapsing sphere, determined for each discretized source time point. The position of the Γ curve within a panel is calculated by testing the panel edges for intersection with the collapsing sphere. If an edge tests positive, then the intersection point is approximated by linear interpolation and after a second edge is found, the location of the Γ curve is complete. The two intersection points are connected by a line segment and the integrands evaluated at the endpoints. Geometric quantities, such as normal vectors and curvatures, are linearly interpolated based on their values at the panel vertices.

Counter-Rotating Predictions

There are several restrictions with regard to counter-rotating propeller (CRP) noise predictions that must be emphasized. It is assumed that both the forward and aft propellers operate at the same angular speed and opposite in direction, have the same number of blades, and their pitch change axes (PCA) are aligned initially (Figure 6).

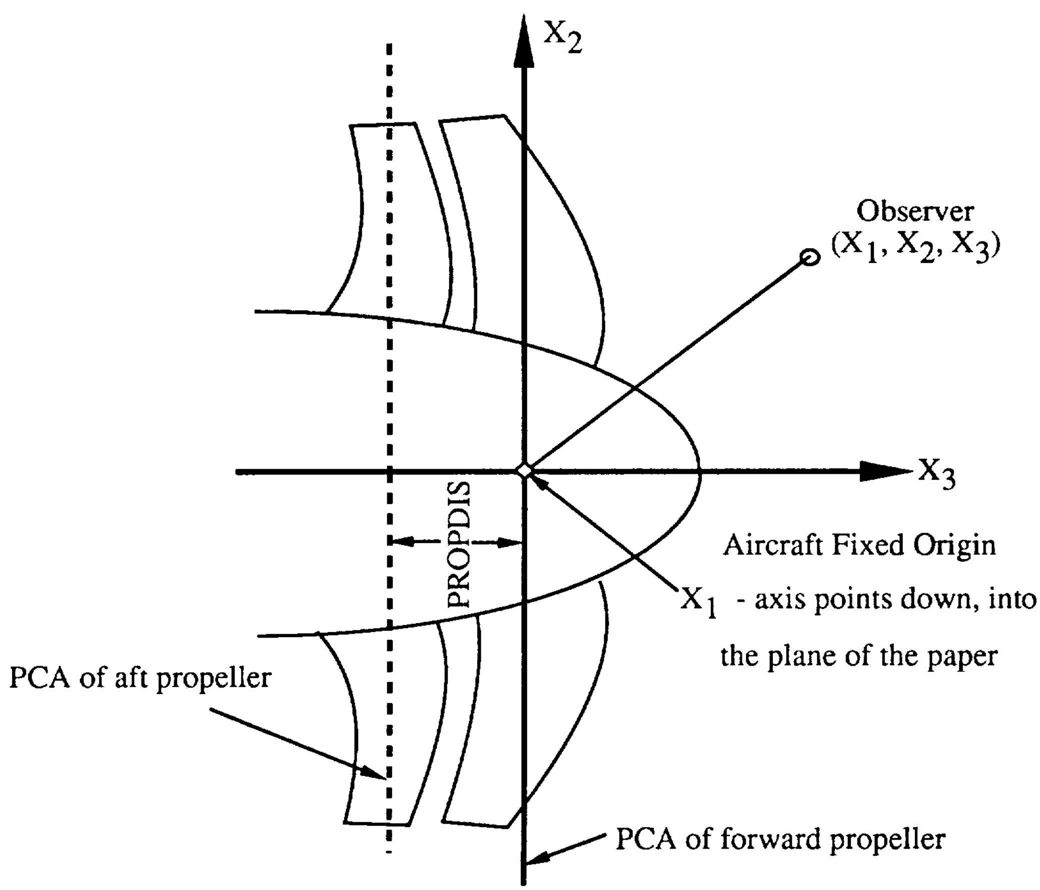

Figure 6. Counter-Rotating Propeller Configuration

These restrictions are imposed to facilitate the spectral analysis of CRP acoustic pressure waveforms. If nonlinear acoustic interactions between the propellers are neglected, then the resultant CRP signal is simply the linear superposition of the individual signals of the two propellers. It is assumed that aerodynamic interactions between the two propellers are accounted for via user supplied blade surface pressure. If the user is interested in CRP predictions where these assumptions cannot be satisfied, then the signals from the individual propellers can be obtained by operating ASSPIN in the single-rotation mode and adding them together in the desired fashion external to ASSPIN. In some instances, ASSPIN can be easily modified to accommodate special circumstances.

A schematic representation of the noise prediction process is shown in Figure 7.

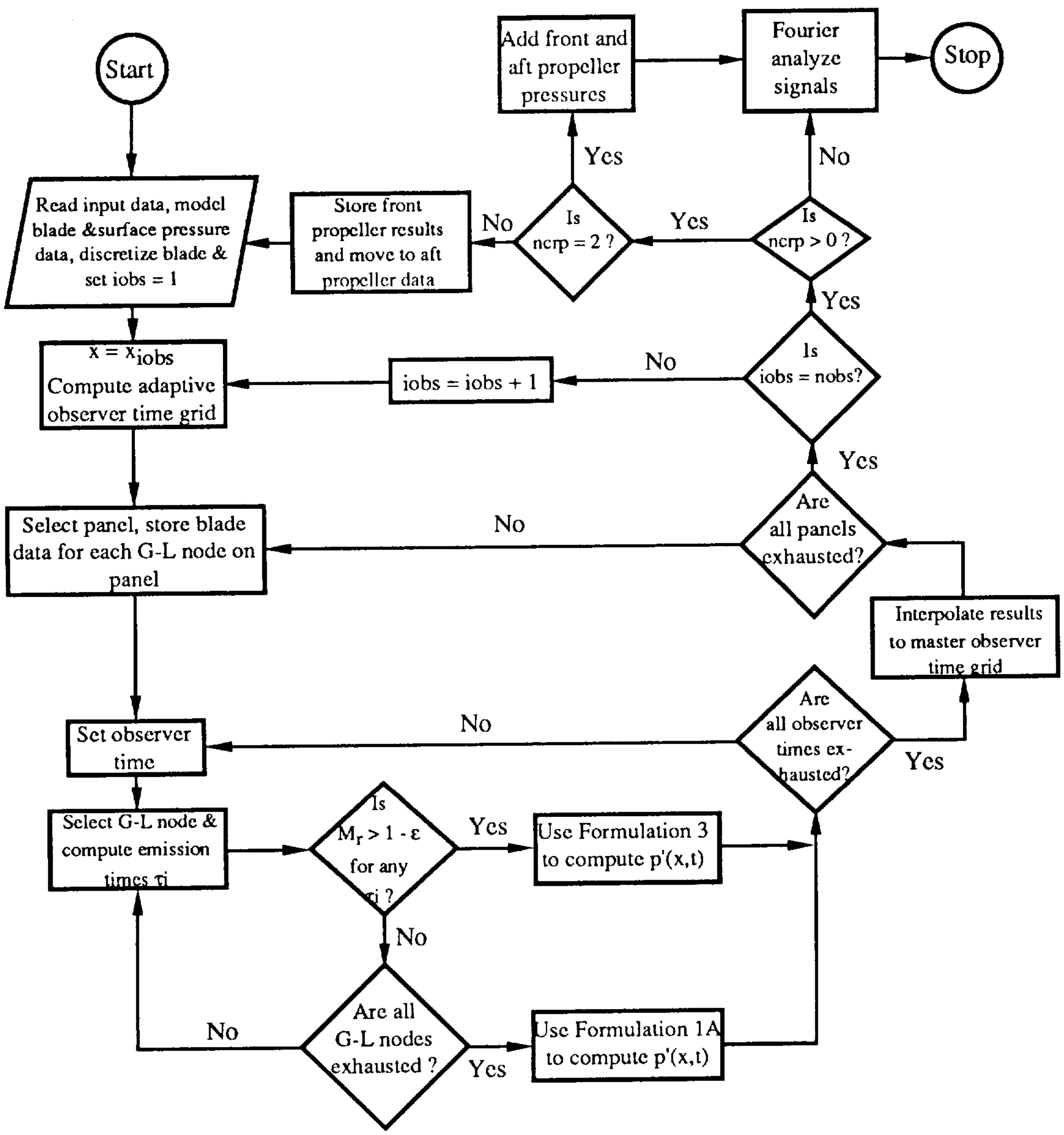

Figure 7. ASSPIN Flowchart

PROGRAM DESCRIPTION

Details of program usage, input specifications, and program output are described in this section.

Operating Instructions

User input consists of a one line identifier, two groups of NAMELIST variables which define operating conditions and grid sizes, blade geometry data, loading data, and observer coordinates. The structure and content of the input file will be discussed in the ensuing subsections. The user input file resides on FORTRAN logical unit number 5.

Standard program output is written to FORTRAN logical unit number 6. Additional output files containing intermediate results must be opened by the user in the calling program. These files are associated with FORTRAN logical unit numbers 7 and 8. ASSPIN output consists of a banner page, a one line identifier, NAMELIST parameters, computational grid information, computed power and thrust coefficients, thickness, loading, and combined noise spectra and signals.

To access ASSPIN, the user's calling program must have the FORTRAN statement

```
CALL ASSPIN( X, NXDIM ).
```

The variable X is a one dimensional dynamic storage array whose dimension, NXDIM, must be at least

$$\max[3 * \mathrm{NOBS} + 9 * \mathrm{NT} + 26 * \mathrm{N1S} * \mathrm{N2S} + 3 * \max(\mathrm{N1S}, \mathrm{N2S}) + 7 * (\mathrm{IGAUSS})^2 + 1,$$
$$\mathrm{NEPTS} * \mathrm{NQPTS} * (5 + 2 * \mathrm{NTPTS}) + 6 * \mathrm{NEPTS} + 2 * \mathrm{NQPTS} + \mathrm{NTPTS}].$$

The capitalized quantities appearing in the above expression are ASSPIN input variables and are defined in the next subsection.

Input Specifications

User input is divided into four categories: 1) physical characteristics of the propeller configuration and ambient medium, 2) grid size parameters for the various numerical schemes, 3) blade geometry and either steady or periodically unsteady blade surface pressure data, and 4) observer coordinates. Details of all user supplied parameters and data are provided below.

NAMELIST PHYSCAL Parameters.

The physical characteristics of the propeller and undisturbed medium are input to ASSPIN via the FORTRAN statement NAMELIST PHYSCAL. In Table 1 below, the NAMELIST PHYSCAL parameters are described. The FORTRAN variable names appear on the left hand side of the table and the variable's definition, type, and units (if applicable) are on the right side of the table.

Table 1. Input Parameter Description - NAMELIST PHYSCAL

VARIABLE	DESCRIPTION
BTIP	Real. Distance, along the PCA, from the propeller axis to the propeller tip in meters.
BINNER	Real. Distance, along the PCA, from the propeller axis to the propeller root section in meters.
VF	Real. Forward flight velocity of propeller in meters per second.
RPM	Real. Propeller angular velocity in revolutions per minute.
C0	Real. Sound speed of undisturbed fluid in meters per second.
RHO0	Real. Density of undisturbed medium in kilograms per cubic meter.
BETA75	Real. Blade angle at 3/4 span in degrees.
NB	Integer. Number of blades.
NOBS	Integer. Number of observers.
STEADY	Logical. STEADY = TRUE $\Rightarrow$ Steady surface pressure. STEADY = FALSE $\Rightarrow$ Unsteady surface pressure.
XINFLOW	Real. Inflow angle in degrees (see Figure 3).
NCRP	Integer. NCRP = 0 $\Rightarrow$ SRP prediction. NCRP = 1 $\Rightarrow$ Front propeller of CRP prediction. NCRP = 2 $\Rightarrow$ Aft propeller of CRP prediction.
PROPDIS	Real. Distance between CRP propellers in meters.

NAMELIST GRID Parameters.

The computational grid sizes are defined by the user through the FORTRAN statement NAMELIST GRID. Grid parameters are defined and their default values and restrictions, if any, are given in Table 2. The effect of varying the grid size parameters has been studied and the results reported in reference 15.

Table 2. Input Parameter Description - NAMELIST GRID

VARIABLE	DESCRIPTION
NT	Integer. Number of observer time points for single blade pressure signature. Restriction: NT $\geq$ 2. Default: NT = 125 * NB.
NS	Integer. Number of sound pressure levels to be output. Default: NS = 30.
N1SUB	Integer. Number of equally spaced spanwise intervals for the subsonic portion of the blade (Figure 4a). Restriction: N1SUB $\geq$ 1. Default: N1SUB = 2.
N1SUP	Integer. Number of equally spaced spanwise intervals for the supersonic portion of the blade (Figure 4a). Restriction: N1SUP $\geq$ 1. Default: N1SUP = 3.
N2SUB	Integer. Number of equally spaced percentage chord intervals for the subsonic portion of the blade (Figure 4a). Restriction: N2SUB $\geq$ 1. Default: N2SUB = 4.
N2SUP	Integer. Number of equally spaced percentage chord intervals for the supersonic portion of the blade (Figure 4a). Restriction: N2SUP $\geq$ 1. Default: N2SUP = 4.
N1S	Integer. Number of equally spaced spanwise points for Formulation 3 panels (Figure 4c). Restriction: N1S $\geq$ 2. Default: N1S = 10.
N2S	Integer. Number of equally spaced percentage chord points for Formulation 3 panels (Figure 4c). Restriction: N2S $\geq$ 2. Default: N2S = 10.
EPSILON	Real. If EPSILON $\geq 1 - M_r$ for some point on a panel then Formulation 3 is used. Default: EPSILON = 0.05
IGAUSS	Integer. Number of Gauss-Legendre nodes used to compute Formulation 1A integrals (Figure 4b). Restriction: IGAUSS $\geq$ 1. Default: IGAUSS = 7.

Blade Geometry and Surface Pressure.

Blade geometry is input by specifying the shape and orientation, with respect to the blade fixed reference frame, of airfoil sections. The number of sections to be input, NEPTS, is determined by the user.

Airfoil sections are generated by cutting the PCA with planes perpendicular to the PCA. The orientation of a section is determined by specifying its distance along the PCA from the propeller axis, η_2, the local chord length, CH, the blade fixed coordinates of the leading edge, η_1^{LE} and η_3^{LE}, and the difference, $\Delta\beta$, between the local blade angle, β, and the blade angle at 75% span, β_{75}. The above measurements are assumed dimensional with distance measured in meters and angles measured in degrees. Note that the innermost cutting plane must be at the spanwise location η_2 = BINNER and the outermost cutting plane is at η_2 = BTIP. These quantities are shown schematically in Figure 8.

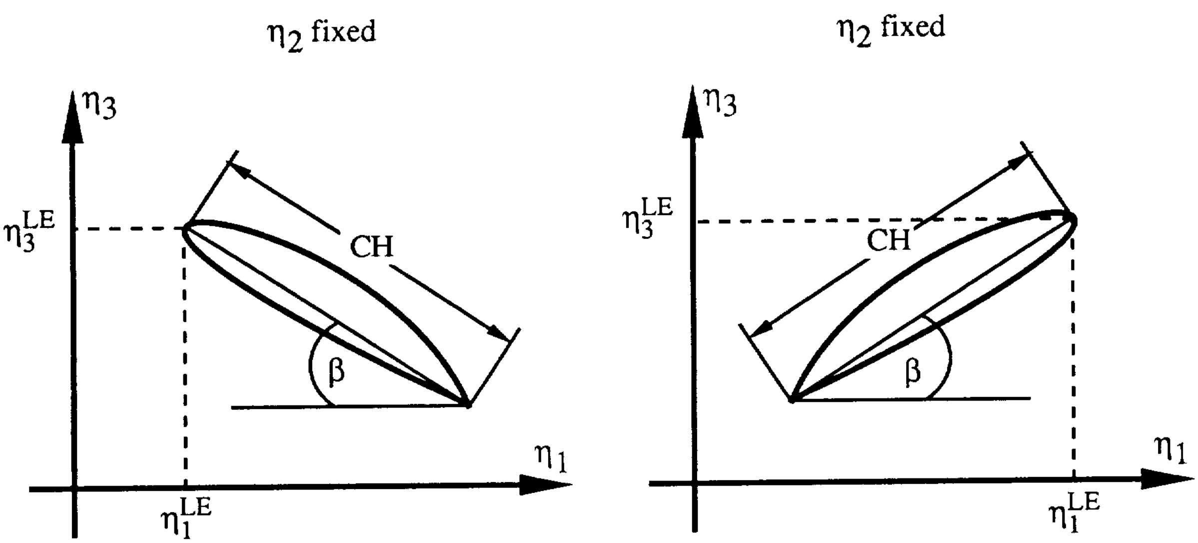

(a) Configuration for SRP and forward propeller of CRP

(b) Configuration for aft propeller of CRP

Figure 8. Airfoil Orientation Specifications

The upper airfoil surface is defined by specifying the distance from the chord line to the upper airfoil surface, y_U, as a function of relative distance along the chord,

Q. By convention, $Q = 0$ corresponds to the leading edge of the section and $Q = 1$ the trailing edge. Also by convention, points lying above the chord line are assigned positive distances, while those lying below the chord line are assigned negative distances. The lower airfoil surface is defined in the same manner. Distance between the chord line and the lower surface is denoted by y_L (see Figure 9). The quantities y_U and y_L are assumed to be nondimensionalized by the user with respect to local chord length. They are input at a discrete number of relative chord points, $\{Q_i\}_{i=1}^{NQPTS}$, which are the same for each section. The leading edge point and the trailing edge point must be included.

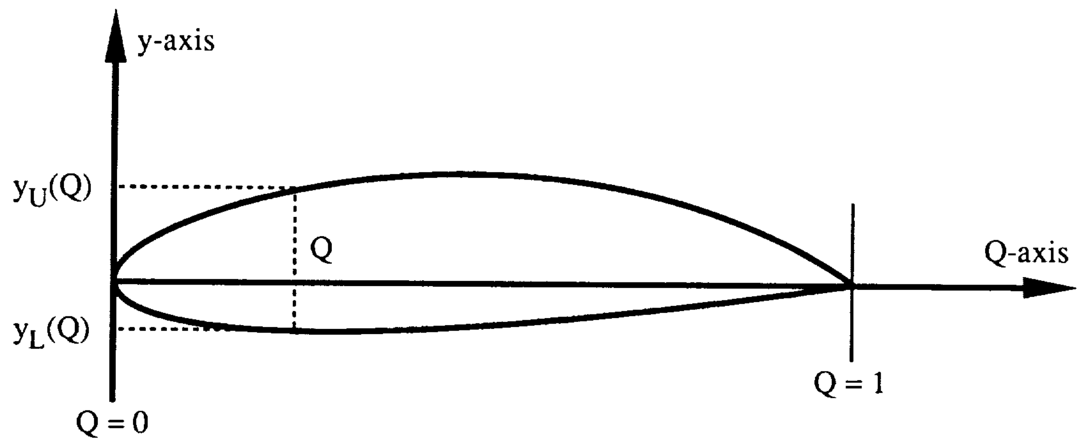

Figure 9. Airfoil Coordinate Specifications

Blade surface pressure must be supplied by the user at each (η_2, Q) point for which blade data is input. The user must nondimensionalize surface pressure by the quantity $\rho_0 \omega^2 (\mathrm{BTIP})^2$. For each spanwise cut, steady surface pressure on both the upper and lower blade surfaces, p_U and p_L respectively, are input as functions of Q.

Unsteady surface pressure is assumed to be periodic with period 2π. The user is responsible for this temporal nondimensionalization. For each blade point, the surface pressure is input as a function of time. Discretized time points, $\{t_i\}_{i=1}^{NTPTS}$, comprising the period are input by the user and must be identical for each blade point. Nondimensionalization of the unsteady surface pressure is the same as for the steady case.

Descriptions of the geometric and surface pressure input parameters are summarized in Table 3.

Table 3. Geometry and Loading Input Parameter Description

VARIABLE	DESCRIPTION
NEPTS	Integer. Number of spanwise data points (airfoil sections). Recommend: 15-30.
NQPTS	Integer. Number of relative chord data points. Recommend: 15-50.
NTPTS	Integer. Number of time points for unsteady pressure data. If STEADY = TRUE, then NTPTS = 1. if STEADY = FALSE, then NTPTS $\geq$ 12. Recommend: 15-50.
Q	Real. Relative chord data points. Nondimensionalized by CH. $Q_1 = 0$ and $Q_{NQPTS} = 1$.
η_2	Real. Spanwise data points in meters. BINNER $\leq \eta_2 \leq$ BTIP.
CH	Real. Local chord length in meters.
$\Delta\beta$	Real. Difference, in degrees, between local blade angle and β_{75}.
η_1^{LE}	Real. η_1 coordinate of leading edge in meters.
η_3^{LE}	Real. η_3 coordinate of leading edge in meters.
y_L	Real. Distance between chord line and lower airfoil surface. Nondimensionalized by CH.
y_U	Real. Distance between chord line and upper airfoil surface. Nondimensionalized by CH.
p_L	Real. Pressure on lower airfoil surface. Nondimensionalized by $\rho_0 \omega^2$ (BTIP)^2.
p_U	Real. Pressure on upper airfoil surface. Nondimensionalized by $\rho_0 \omega^2$ (BTIP)^2.
t	Real. Time points for unsteady surface pressure. Nondimensionalized by $2\pi/\omega$. $t_1 = 0$ and $t_{NTPTS} = 2\pi$.

Observer Coordinates.

The acoustic observers are assumed to translate with the aircraft. Their coordinates are expressed in meters and are specified by the user with respect to the aircraft fixed reference frame.

Input File Structure

The order and format of the user supplied input file is discussed in this subsection. Both SRP and CRP predictions are considered. Examples involving both cases appear in the next section.

SRP Predictions.

1. 80 character identifier - FORMAT(1X,A80).
2. NAMELIST PHYSCAL - NCRP = 0 for SRP Predictions.
3. NAMELIST GRID.
4. Blade coordinates and surface pressure data.

4a. NEPTS, NQPTS, NTPTS - FORMAT(1X, 3I10).

4b. Relative chord grid - FORMAT(1X, E15.7).

$$Q_1 = 0.0$$
$$\vdots$$
$$Q_{NQPTS} = 1.0$$

4c. η_2, CH, $\Delta\beta$, η_1^{LE}, η_3^{LE} - FORMAT(1X, 5E15.7).

$y_L(Q_1)$, $y_U(Q_1)$, $p_L(Q_1)$, $p_U(Q_1)$ - FORMAT(1X, 4E15.7).

$$\vdots$$

$y_L(Q_{NQPTS})$, $y_U(Q_{NQPTS})$, $p_L(Q_{NQPTS})$, $p_U(Q_{NQPTS})$ - FORMAT(1X, 4E15.7).

The quantities p_L and p_U refer to steady blade pressure. If the blade loads are unsteady, then ASSPIN does not use p_L and p_U. However, properly formatted numbers must appear in these locations.

Item 4c. is repeated for each of the NEPTS airfoil sections.

4d. Time point grid for unsteady surface pressure - FORMAT(1X, 5E13.6).

READ(5)(T(K), K = 1,NTPTS)

T(1) = 0.0, ..., T(NTPTS) = 2π.

If STEADY = TRUE, then 4d. is omitted.

4e. Unsteady surface pressure - FORMAT(1X, 5E13.6).

DO K = 1,NTPTS

DO I = 1,NEPTS

READ(5)(p_L(I,J,K), J = 1,NQPTS)

READ(5)(p_U(I,J,K), J = 1,NQPTS)

If STEADY = TRUE, then 4e. is omitted.

5. Observer coordinates - Unformatted.

READ(5,*)(($\vec{x}$(I,J), J = 1,3), I = 1,NOBS)

$\vec{x}$(I,J) is the J-th Cartesian component, with respect to the aircraft fixed frame, of the I-th observer.

CRP Predictions.

1. 80 character identifier - FORMAT(A80).
2. NAMELIST PHYSCAL for forward propeller - NCRP = 1.
3. NAMELIST GRID for forward propeller.
4. Blade coordinates and surface pressure data for forward propeller.

   See format and instructions for SRP predictions.
5. Observer coordinates.

   See format and instructions for SRP predictions.

   The origin of the aircraft fixed frame is assumed to be at the hub center of the forward propeller (see Figure 6).
6. NAMELIST PHYSCAL for aft propeller - NCRP = 2.

   NOBS and NB are the same for both propellers. RPM for the aft propeller must be the negative of RPM for the forward propeller.
7. NAMELIST GRID for aft propeller.

   NT must be the same for both propellers.

8. Blade coordinates and surface pressure data for aft propeller.

   See format and instructions for SRP predictions.

9. Observer coordinates.

   See format and instructions for SRP predictions.

   This information must be the same as for the forward propeller.

EXAMPLES

Three sample calculations that demonstrate the capabilities of ASSPIN are presented in this section. In each example, the operating conditions and acoustic results are displayed. The source code and input and output files for the three cases can be obtained upon request. The authors can be reached at the email address mhd@sabre.larc.nasa.gov.

SRP Prediction with Axial Inflow

In this example, the noise generated by the SR-7L propeller (reference 16) was computed. The propeller is eight bladed, has a diameter of nine feet, and is designed to cruise at Mach 0.8. The NAMELIST PHYSCAL are as follows:

BTIP = 1.3716,
BINNER = 0.3429,
VF = 239.4,
RPM = 1679.0,
C0 = 299.3,
RHO0 = 0.372,
BETA75 = 57.0,
NB = 8,
NOBS = 1,
STEADY = TRUE,
XINFLOW = 0.0,
NCRP = 0,
PROPDIS = 0.0.

The acoustic observer is located 0.62 diameters from the propeller tip and 0.25 diameters aft of the propeller plane. The coordinates of the observer with respect to the aircraft fixed frame are (0.0, 3.06, -0.686). The NAMELIST GRID parameters are set to their default values (see Table 1). Aerodynamic loads were computed with the Adamczyk code (reference 17).

The computed thrust and power coefficients for this example are $C_T = 0.53$ and $C_P = 1.85$, respectively. Acoustic waveforms and spectra for the thickness, loading, and combined noise are shown in Figure 10.

SRP Prediction with Nonaxial Inflow

The SR-7L propeller was again used for this case. The propeller was set at an inflow angle of 4.6 degrees and the unsteady blade loads were computed with the Whitfield code (reference 18). The NAMELIST PHYSCAL parameters are as follows:

BTIP = 1.3716,
BINNER = 0.3429,
VF = 239.4,
RPM = 1679.0,
C0 = 299.3,
RHO0 = 0.372,
BETA75 = 57.8,
NB = 8,
NOBS = 1,
STEADY = FALSE,
XINFLOW = 4.6,
NCRP = 0,
PROPDIS = 0.0.

The acoustic observer is the same as in the previous case. ASSPIN grid parameters were again set to their default values.

The computed thrust and power coefficients for this case are $C_T = 0.43$ and $C_P = 1.75$, respectively. Acoustic waveforms and spectra for the noise components are displayed in Figure 11.

CRP Prediction with Axial Inflow

The results computed here were produced by a model counter-rotation propeller system. The blade loading, which includes the aerodynamic interaction, was obtained from Adamczyk's code. For the forward propeller, the NAMELIST PHYSCAL parameters are as follows:

BTIP = 0.3064,
BINNER = 0.137,
VF = 242.9,
RPM = 8283.0,
C0 = 338.3,
RHO0 = 1.039,
BETA75 = 56.3,
NB = 8,
NOBS = 1,
STEADY = TRUE,
XINFLOW = 0.0,
NCRP = 1,
PROPDIS = 0.1037,

and for the aft propeller:

BTIP = 0.2973,
BINNER = 0.1322,
VF = 242.9,
RPM = -8283.0,
C0 = 338.3,
RHO0 = 1.039,
BETA75 = 53.9,
NB = 8,
NOBS = 1,
STEADY = TRUE,
XINFLOW = 0.0,
NCRP = 2,
PROPDIS = 0.0.

The acoustic observer is located 1.62 diameters from the forward propeller tip and slightly aft of the propeller plane of the forward propeller. The coordinates of the observer with respect to the aircraft fixed frame are (0.8, 0.0, -0.05).

The computed thrust and power coefficients for the forward propeller are $C_T = 0.34$ and $C_P = 1.25$, and for the aft propeller $C_T = 0.39$ and $C_P = 1.36$. Acoustic results for this case appear in Figure 12.

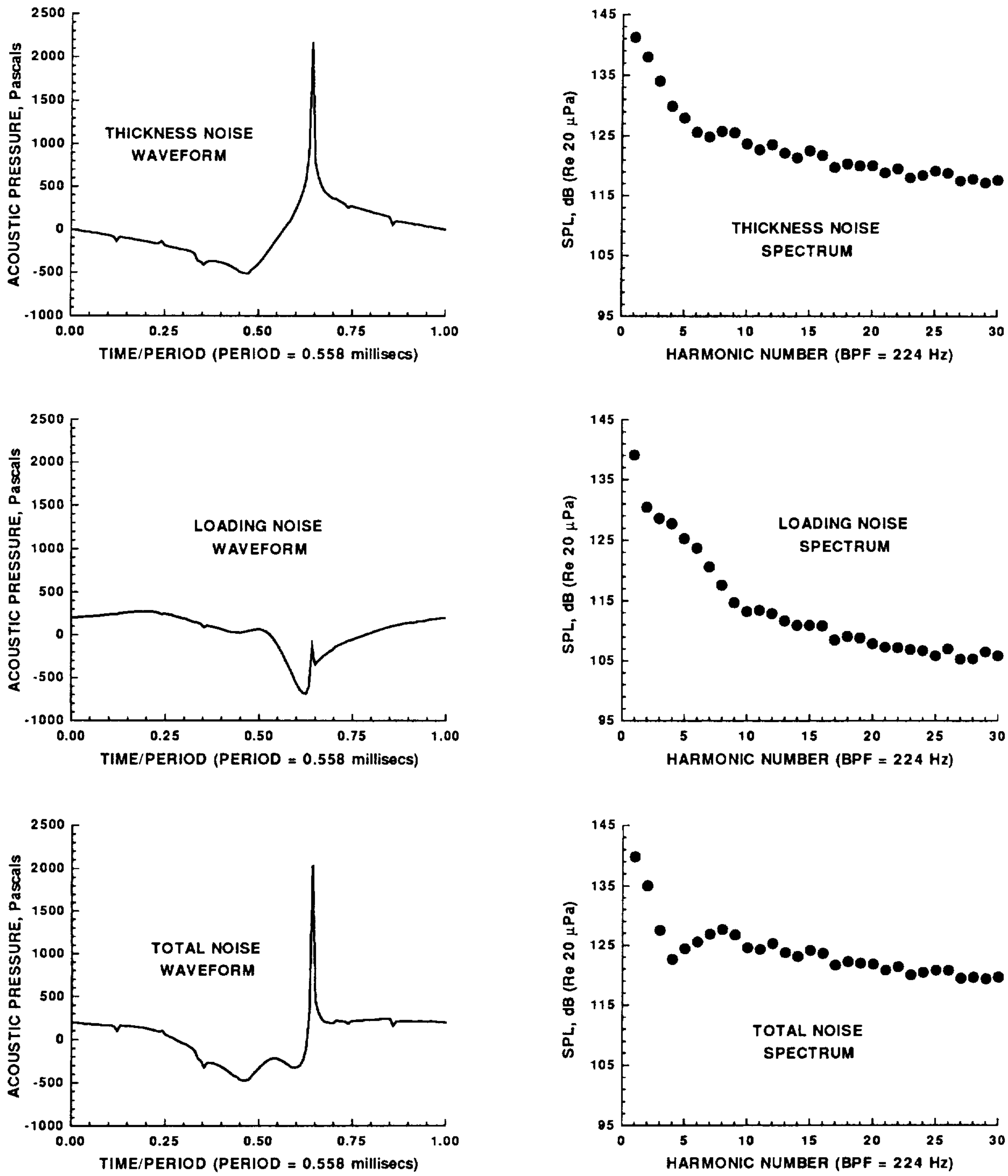

Figure 10. Acoustic Results for SRP with Axial Inflow

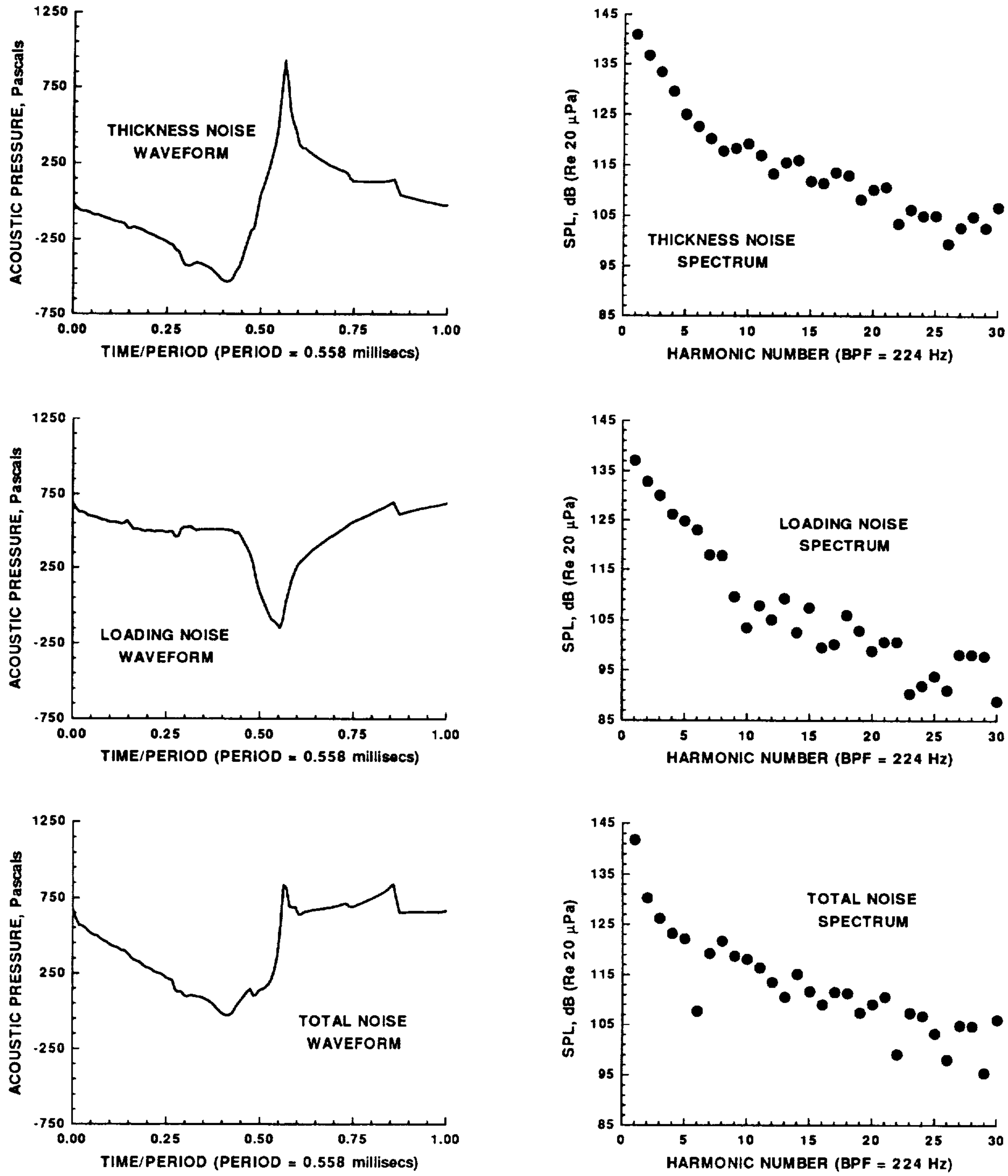

Figure 11. Acoustic Results for SRP with Nonaxial Inflow

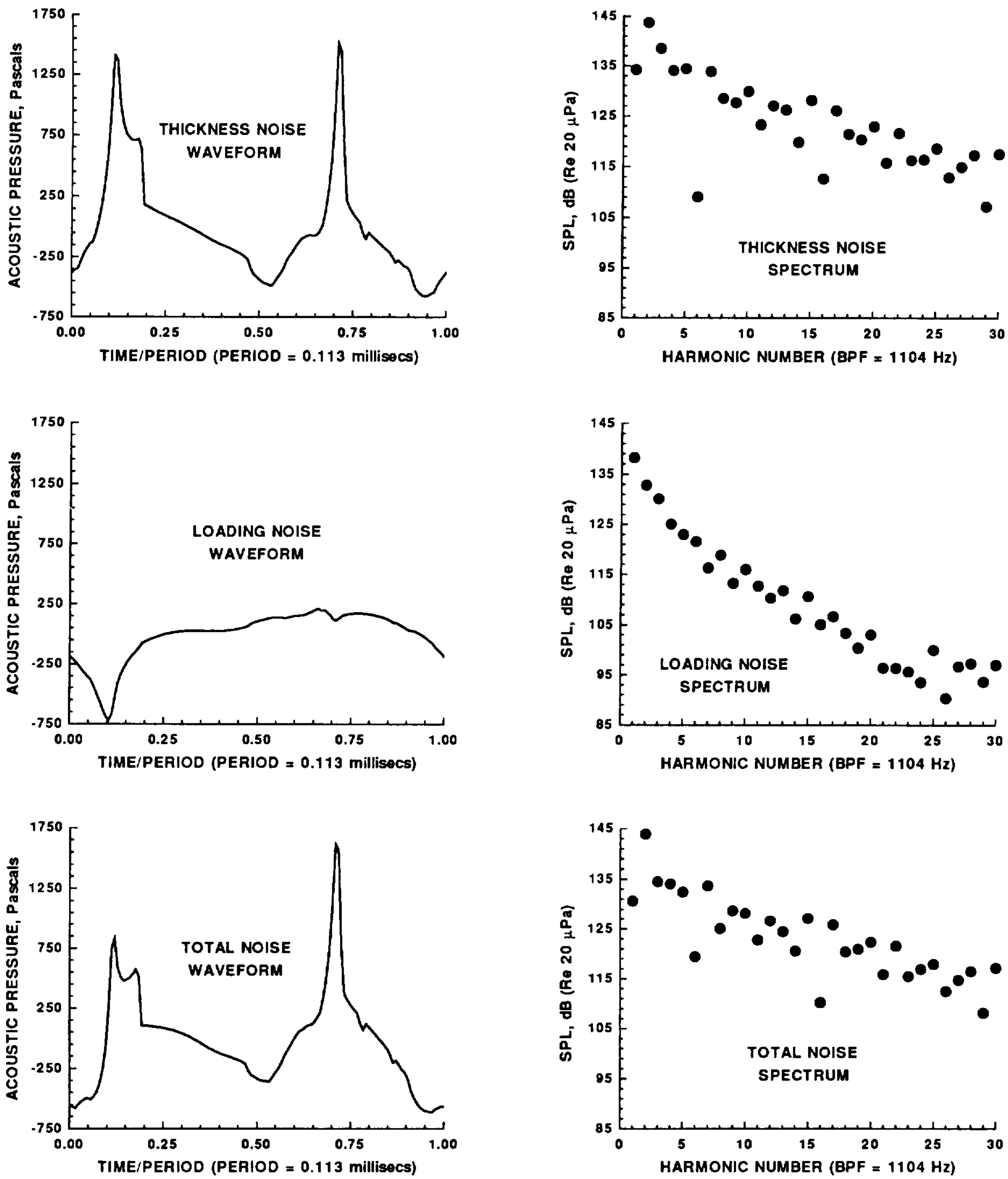

Figure 12. Acoustic Results for CRP with Axial Inflow

CONCLUSIONS

The computer code ASSPIN predicts the noise produced by advanced technology propellers in either the single-rotation or counter-rotation mode. It is based on two theoretical formulations of Farassat, which are valid in the near and far fields and for axial and nonaxial inflow conditions. One formulation is valid for subsonic helical tip speeds and involves integrals over the surface of a propeller blade. The other is used for transonic and supersonic helical tip speeds and is written as surface and line integrals over the acoustic planform, generated by the blade, and its boundary.

Efficient computational algorithms are used in ASSPIN to evaluate the theoretical formulations numerically. Blade geometry and surface pressure data are approximated by high order splines. Accurate numerical integration schemes and an adaptive observer time grid have been developed to reduce computer execution time. The most computationally intensive portion of ASSPIN involves the accurate calculation of retarded times. In a typical noise prediction, the retarded time equation must be solved about 500,000 times and in some instances has multiple solutions. ASSPIN employs an exhaustive root finding procedure which accurately calculates the retarded times in a few iterations.

Details on the use of ASSPIN are given in this paper. Input to ASSPIN consists of operating conditions, observer coordinates, and blade geometry and surface pressure data. ASSPIN produces acoustic signatures and spectra of thickness, loading, and overall noise.

REFERENCES

1. Arndt, W. E.: Propfans Go Full Scale. Aerospace America, 1984, pp. 100-103.
2. Farassat, F. and Succi, G. P.: The Prediction of Helicopter Rotor Discrete Frequency Noise. Vertica, Vol. 7, 1983, pp. 309-320.
3. Farassat, F.: Theoretical Analysis of Linearized Acoustics and Aerodynamics of Advanced Supersonic Propellers. AGARD-CP-366 (10), 1985, pp. 1-15.
4. Martin, R. M. and Farassat, F.: Users' Manual for a Computer Program To Calculate Discrete Frequency Noise of Conventional and Advanced Propellers. NASA TM-83135, 1981.
5. Zorumski, W. E. and Weir, D. S., editors: Aircraft Noise Prediction Program (ANOPP) Theoretical Manual - Propeller Aerodynamics and Noise. NASA TM-83199, Pt 3, 1986.

6. Dunn, M. H. and Tarkenton, G. M.: Users' Manual for the Langley High Speed Propeller Noise Prediction Program (DFP-ATP). NASA CR- 4208,1989.
7. Dunn, M. H. and Farassat, F.: State-of-the-Art of High Speed Propeller Noise Prediction - A Multidisciplinary Approach and Comparison with Measured Data, AIAA paper 90-3934, 1990.
8. Farassat, F.: Discontinuities in Aerodynamics and Aeroacoustics: The Concept and Application of Generalized Derivatives. Journal of Sound and Vibration, Vol. 55, 1977, pp. 165-193.
9. Ffowcs Williams, J. E. and Hawkings, D. L.: Sound Generation by Turbulence and Surfaces in Arbitrary Motion. Philos. Trans. Royal Soc. London, ser. A, Vol. 264, no. 1151, May 8, 1969, pp. 321-342.
10. Farassat, F.: Theory of Noise Generation From Moving Bodies With an Application to Helicopter Rotors. NASA TR R-451, 1975.
11. Conte, S. D. and de Boor, C.: Elementary Numerical Analysis an Algorithmic Approach, Second Edition. McGraw-Hill Book Co., New York, 1972.
12. de Boor, C.: A Practical Guide to Splines. Springer-Verlag, New York, 1978.
13. Dunn, M. H.: The Solution of a Singular Integral Equation Arising from a Lifting Surface Theory for Rotating Blades, PhD Dissertation, Old Dominion University, 1991.
14. Mathematical and Statistical Software at Langley. Central Scientific Computing Complex Doc. N2-3d, NASA Langley Research Center, May 1990.
15. Farassat, F., Dunn, M. H. and Padula, S.: Advanced Turboprop Noise Prediction Based on Recent Theoretical Results, Journal of Sound and Vibration, Vol. 119, 1987, pp. 53-79.
16. DeGeorge, C. L.: Large-Scale Advanced Propfan Final Report, NASA CR-182112, 1988.
17. Celestina, M. L., Mulac, R. A. and Adamczyk, J. J.: A Numerical Simulation of the Inviscid Flow through a Counter-Rotating Propeller, Transactions of the ASME, Journal of Turbomachinery, Vol. 108, 1986, pp. 187-193.
18. Whitfield, D. L., Swafford, T. W., Janus, J. M., Mulac, R. A. and Belk, D. M.: Three Dimensional Unsteady Euler Solutions for Propfans and Counter-Rotating Propfans, AIAA-87-1197, 1987.

REPORT DOCUMENTATION PAGE

Form Approved
OMB No 0704-0188

1. AGENCY USE ONLY *(Leave blank)*

2. REPORT DATE
April 1992

3. REPORT TYPE AND DATES COVERED
Contractor Report

4. TITLE AND SUBTITLE
Computational Methods in the Prediction of Advanced Subsonic and Supersonic Propeller Induced Noise - ASSPIN Users' Manual

5. FUNDING NUMBERS
C NAS1-19000

WU 535-03-11-02

6. AUTHOR(S)
M. H. Dunn and G. M. Tarkenton

7. PERFORMING ORGANIZATION NAME(S) AND ADDRESS(ES)
Lockheed Engineering & Sciences Company
144 Research Drive
Hampton, VA 23665-5225

8. PERFORMING ORGANIZATION REPORT NUMBER

9. SPONSORING/MONITORING AGENCY NAME(S) AND ADDRESS(ES)
National Aeronautics and Space Administration
Langley Research Center
Hampton, VA 23665-5225

10. SPONSORING/MONITORING AGENCY REPORT NUMBER
NASA CR-4434

11. SUPPLEMENTARY NOTES
Langley Technical Monitor: F. Farassat

12a. DISTRIBUTION/AVAILABILITY STATEMENT
Unclassified - Unlimited

Subject Category 71

12b. DISTRIBUTION CODE

13. ABSTRACT *(Maximum 200 words)*

This document describes the computational aspects of propeller noise prediction in the time domain and the use of the high speed propeller noise prediction program ASSPIN (Advanced Subsonic and Supersonic Propeller Induced Noise). The code, which was formerly called DFP-ATP (Dunn-Farassat-Padula Advanced Technology Propeller Noise Prediction Program), was developed at NASA Langley Research Center (LaRC) by the authors and F. Farassat and S. Padula of NASA LaRC. ASSPIN is the latest version of a sequence of propeller noise prediction codes that are based on the theoretical formulations of Farassat (references 1-3). ASSPIN incorporates full surface formulations, advanced blade geometry modelling, and relative to the previous version (reference 3), contains enhanced numerical algorithms that result in reduced computational time. In addition, the ability to treat the nonaxial case has been included.

14. SUBJECT TERMS
Advanced technology propellers; Supersonic propellers; aeroacoustics; Ffowcs Williams-Hawkings equation; Computational techniques

15. NUMBER OF PAGES
44

16. PRICE CODE
A03

17. SECURITY CLASSIFICATION OF REPORT	18. SECURITY CLASSIFICATION OF THIS PAGE	19. SECURITY CLASSIFICATION OF ABSTRACT	20. LIMITATION OF ABSTRACT
Unclassified	Unclassified		

National Aeronautics and
Space Administration
Code JTT
Washington, D.C.
20546-0001

Official Business
Penalty for Private Use, $300

BULK RATE
POSTAGE & FEES PAID
NASA
Permit No. G-27

NASA

POSTMASTER: If Undeliverable (Section 158 Postal Manual) Do Not Return